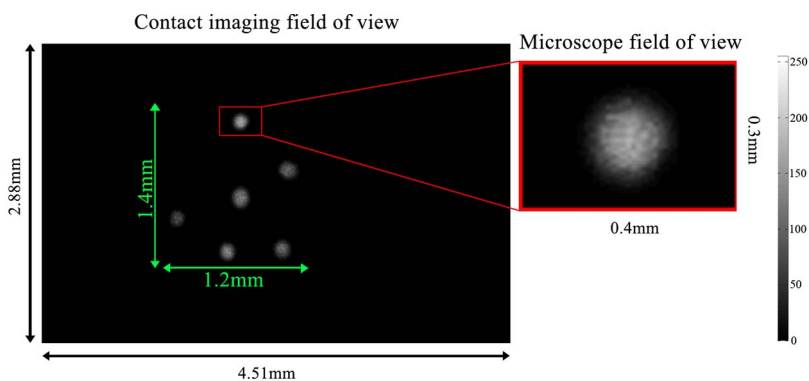# A Novel Lensless Miniature Contact Imaging System for Monitoring Calcium Changes in Live Neurons

Volume 6, Number 1, February 2014

Anil Kumar Mudraboyina
Lior Blockstein
Collin C. Luk
Naweed I. Syed
Orly Yadid-Pecht, Fellow, IEEE

Contact imaging field of view

Microscope field of view

2.88mm

1.4mm

1.2mm

4.51mm

0.3mm

0.4mm

IEEE

A Novel Lensless Miniature Contact Imaging System for Monitoring Calcium Changes in Live Neurons

Anil Kumar Mudraboyina,[*1] **Lior Blockstein,**[*1] **Collin C. Luk,**[2] **Naweed I. Syed,**[2] **and Orly Yadid-Pecht,**[1] *Fellow, IEEE*

[1]University of Calgary, Department of Electrical and Computer Engineering,
Calgary, AB T2N 1N4, Canada
[2]Hotchkiss Brain Institute, Faculty of Medicine, University of Calgary, Calgary, AB T2N 4N1, Canada

Abstract: Here, we report on the design, fabrication, and verification of a novel CMOS-imager-based contact imaging system. We acquired fluorescent images from live neurons by monitoring calcium changes with Fura-2 dye. Our current device consists of a removable absorption filter interfaced with a CMOS imaging sensor and an external DG-4 lamp for excitation. Fura-2 loaded *Lymnaea stagnalis* neurons were stimulated with dual excitation wavelengths of 340 and 380 nm; our image sensor detected 510-nm emission. We show that our system is capable of detecting intracellular calcium changes in Fura-2 loaded neurons. Further, this sensor also enabled viewing of multiple neurons over a large surface area simultaneously, an option that is not readily available in conventional light microscopy.

Index Terms: Contact Imaging, fluorescence, Fura-2 AM, fluorescent contact imaging.

1. Introduction

Non-invasive monitoring/imaging of neuronal activity at multiple locations is central to deciphering brain function under normal and various pathological conditions. This is currently achieved through conventional microscopy approaches with cumbersome optical components such as lenses, prisms, filters and a high precision microscope body that coordinate these components. These conventional optical components are located between the specimen of interests and either the observer, or a camera to capture the image. Due to these intermediate optical components, such systems are generally large, expensive and immobile. These current constraints hinder conventional microscopy from becoming highly portable for neuronal imaging, which remains expensive to install and operationalize.

Contact imaging is a new method of micro imaging where the sample of interest is interfaced directly with the sensor array. The image is acquired by projecting light through the coupled sample or by capturing the light emitted by the sample. This approach eliminates several intermediate optical components that are required in conventional microscopy. While conventional imaging continues to provide better spatial resolution, contact imaging offers other advantages such as better light collection efficiency [1]–[3] lower cost, reduced weight and size, low power requirements and portability.
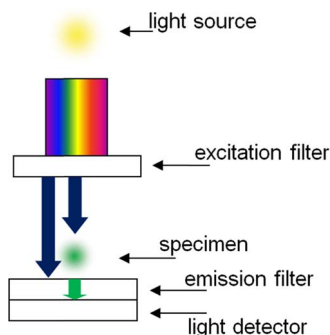
Fig. 1. A schematic diagram of the contact imaging system. In a contact imaging system, the emission filter is coupled with the light detector and the specimen is then cultured directly on the filter. The excitation light is blocked by the emission filter, but allows for the passage of emitted light from the specimen which is detected by the light detector.

Contact imaging can be used for different types of spectroscopy such as absorption [4] and fluorescence [5]. Fluorescence spectroscopy is widely used as an imaging method in biological, pharmaceutical and medical research fields [5]–[14]. It utilizes light to excite fluorophores, which re-emit an emission light. Typically the intensity of the emission light is 10^{-4} to 10^{-6} [15], [16] times the excitation light. Therefore in fluorescence spectroscopy, an emission filter between the sample and the sensor is required to block excitation light and transmit emission light [17]. Similarly, in contact imaging systems, the filter is manufactured on top of the sensor and the sample is placed on top of the filter. To acquire a fluorescent image from the sample, the sensor array is illuminated by a uniform excitation light.

In this current study, a previously reported Polyvinyl acetate (PVAc) Benzophenone-8 (PVAcB-8) filter [17] was manufactured on top of the sensor array of a CMOS image sensor (CIS). In addition to its simple design and fabrication process, the filter can also be easily removed from the sensor therefore allowing reusability of the sensors. In this manuscript, Section 2 reviews the filter manufacturing method, Section 3 describes the system's quantum efficiency (QE) before and after the filter is applied, Section 4 tests the system's response to repetitive usage, Section 5 shows fluorescence detection of fluorescent micro beads and its repeatability, Section 6 reports the test results when applied to *Lymnaea stagnalis* neurons, Section 7 shows the spatial resolution limit of our system, and Section 8 summarizes the conclusions.

2. System Design and Manufacturing

The schematic of a contact imaging system is shown in Fig. 1. The system's light path is similar to that reported previously [18]–[20]. However unlike previous works, this system is designed for fluorescent imaging via two excitation wavelengths, 340 nm and 380 nm. This is important because it allows the monitoring of intracellular $[Ca^{2+}]$ variation in Fura-2 loaded neurons. Additionally, the system design includes an easily removable PVAc based filter allowing for reuse of these sensors.

In this section the components of the fluorescent contact imaging system are described from the bottom up. The light detector used in the system is Aptina MT9V032 CIS. Aptina MT9V032 CIS has been chosen mainly due to its low light detection ability (sub 0.1 lux) and monochrome design. No Bayer filter allows us to fully control the wavelengths detected by the sensor when manufacturing our filter on top of the sensor array. The CIS mounted on a FPGA board (part number UI-1222LE-M-GL) was purchased from 1stVision Inc. [shown in Fig. 2(a)]. The size of the FPGA board is 36 × 36 × 8 mm (HxWxD). The sensor package cross section is shown in Fig. 2(b), it is a sealed package with a glass lid (borosilicate glass) cover above the sensor which protects the sensor from external hazards and prevents contact [21]. For our purposes, the borosilicate glass was removed to gain access to the sensor. Package cross section after glass removal is shown in Fig. 2(c). This step is required due
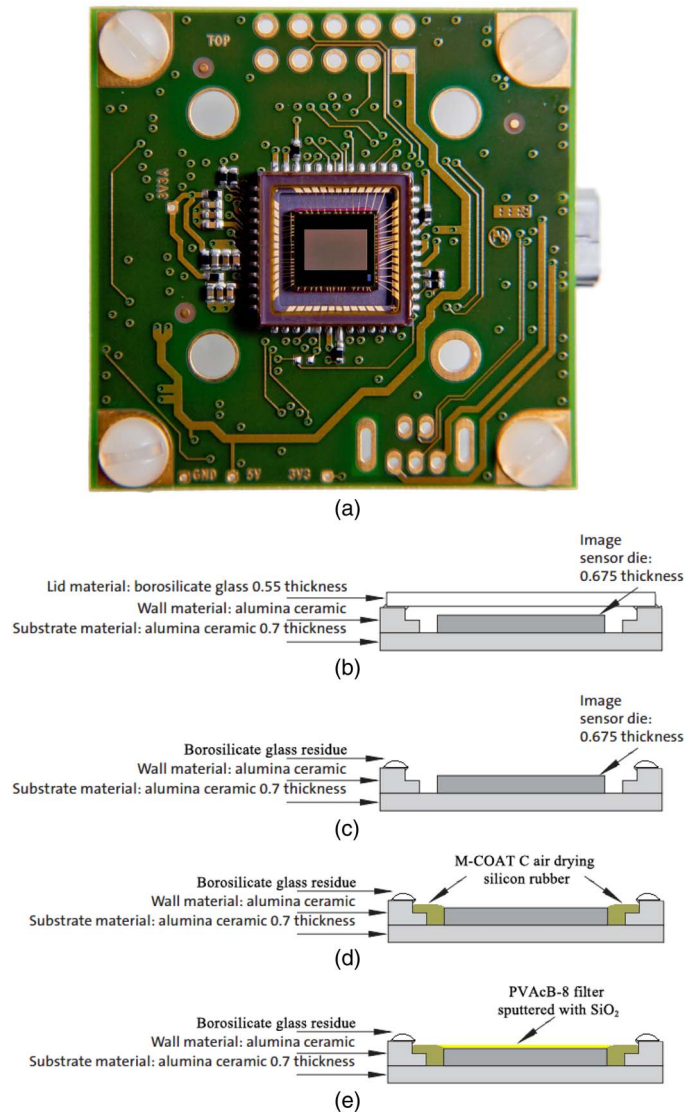
Fig. 2. The image sensor used is an (a) Aptina MT9V032 CIS mounted on FPGA board [21]. A cross-section of the package shows the original image sensor (b) with glass lid attached, and then with the (c) glass lid removed. With the glass is removed, to protect the wire bonding, (d) silicon rubber is applied. Finally, the (e) PVAcB-8 filter is spin coated onto the surface of the sensor and a layer of SiO_2 is sputtered.

to the packaging method chosen by Aptina. In future work, we aim to use our custom designed low light CMOS sensor (which will not have a glass lid) [22], [23].

The MT9V032 is packaged in a standard wire bonding package. The wire bonding is a common method for bonding the sensor die to the packaging, it utilizes micro-wires that are 30 microns in diameter and can be easily severed by touch. In order to protect the bond wires they were covered via M-COAT C air drying silicon rubber; purchased from InterTechnology Inc. The silicone rubber was applied to the wire bonding area and allowed to dry for a period of 24 hours. Sensor-cross section after silicon rubber application is shown in Fig. 2(d). Upon drying, the silicon rubber hardens and creates a protective shell [22], [23]. With the wire bonds protected it is possible to safely apply an emission filter on to the sensor array.

In fluorescent imaging, the emission filter is of high importance since it is responsible for the signal-to-noise ratio (SNR) of the excitation/emission light. By attenuating the excitation light the filer

shifts the SNR in favor of emission light. The different properties of the manufactured PVAcB-8 filter were described and demonstrated in a previous work [17]. Specifically it has been demonstrated that PVAcB-8 filter thickness of 20 μm is efficient in blocking the excitation light while transmitting the emission light from Fura-2. The emission PVAcB-8 filter was manufactured on top of the sensor array via spin coating. The spin coating speed was calibrated to achieve a filter thickness of 20 μm. A cross section of the sensor after filter application is shown in Fig. 2(e). To achieve the desired thickness, an empirical method was used. A filter was manufactured on top of the sensor array via different spin coating speeds. The thickness of the filter was measured and recorded as a function of the spin coating speed and the results were fitted to an exponential function. By using the fitted equation, the spin speed was determined to be 800 RPM in order to achieve the desired thickness. After spin coating, the manufactured filter on the sensor was allowed to dry for a period of 24 hours. After the drying period the sensor was loaded into a sputtering device (Lesker CMS-18) and the filter was coated with a 100 nm layer of SiO_2 via sputtering. The SiO_2 layer has been deposited in order to mimic the normal glass slide culture conditions in a petri dish. We found this improved culture and dye loading conditions (data not shown).

It is important to note that the PVAcB-8 filter was manufactured on top of the MT9V032, which is packaged and attached to a FPGA board. When compared to other published work, the filter is often manufactured separately and subsequently attached to the sensor [19], [20] [24]–[28]. Such manufacturing method results in an increase in filter thickness. This parameter can significantly affect the image [1], [19], [20] as the filter thickness is inversely correlated to the system's light collection and resolving power. Therefore, it is best to keep the filter thickness as low as possible. In addition, some reported work do not provide the method used to manufacture emission filters on the sensor arrays, nor does it provide the filter thickness [18], [29], therefore making direct comparison impossible.

The authors are unaware of any published work that describes a manufacturing method of an emission filter on a packaged sensor with an attached FPGA board. Thus the described manufacturing method is optimal when compared to other work. It demonstrates that the filter can be manufactured on commercially available or custom made sensors even after the sensor die has been packaged and even if the sensor has been attached to an FPGA board.

For the excitation light, a Lambda DG-4 illumination system was used. The illumination system utilizes 150W xenon lamp and a dichroic filter in order to select the desired wavelengths. For 340 nm excitation light, an Asahi Spectra XBPA340 band pass filter was used. For 380 nm excitation light, a ThorLabs FB380-10 band pass filter was used. Lambda DG-4 is the largest component of the system with dimensions 48 × 25 × 25 cm (H × W × D) and a weight of 20 kg. Despite the use of a larger excitation lamp system, the main goal of this specific study was to reduce the capturing part of the imaging system.

3. System Testing for Quantum Efficiency

Quantum efficiency (QE) measurement of the system is necessary to test the system's ability to block the excitation wavelength. Fura-2 is a ratiometric dye and has two excitation peaks corresponding to calcium bound molecules at 335 nm and calcium free at 362 nm. However the excitation wavelengths used for Fura-2 are 340 nm for calcium bound and 380 nm for calcium free. The large shift from 362 nm to 380 nm is due to consideration of signal to noise ratio (SNR). Emission originated from excitation at 362 nm will be composed of strong fluorescence originated from calcium free Fura-2 as well as calcium bound Fura-2. Excitation at 380 nm is more favorable because the emission signal will be composed mostly of calcium free Fura-2 signal, therefore increasing the SNR. For successful fluorescent imaging, the manufactured fluorescence filter must block both 340 nm and 380 nm wavelengths.

The QE of Aptina MT9V032 CIS was measured for wavelengths ranging from 300 nm to 600 nm in steps of 10 nm, before and after the filter application on the sensor array. To measure the response curve, an Oriel Monochromator model 77700 was used. The exit light from the monochromator was collimated and made uniform and projected on the sensor array. The results of the calculated QE as a function of wavelength, before and after filter fabrication are presented in Fig. 3.
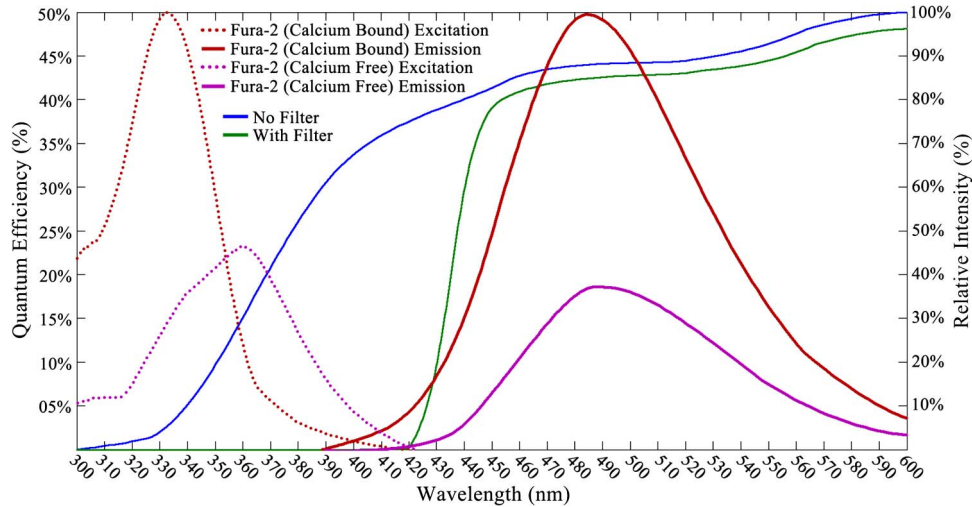
Fig. 3. The graph demonstrates Fura-2 excitation and emission spectra in terms of relative intensity (%) and the quantum efficiency (%) curve of the Aptina MT9V032 sensor with and without the PVAcB-8 emission filter. As shown in the graph, the filter effectively blocks the transmission of Fura-2 excitation wavelength for both the bound and unbound state.

Additionally the excitation and emission spectra of Fura-2 fluorescent dye was overlaid on to the sensor QE curve, and it is also presented in Fig. 3 in percentage. It can be seen from Fig. 3 that the PVAcB-8 filter performs well in blocking both 340 nm and 380 nm wavelengths used for Fura-2 excitation, as well as blocking all other wavelengths up to 420 nm. These results are consistent with previous work [17].

4. System Testing for Repetitive Usage

To test whether the sensor's sensitivity was consistent over repeated application and removal of the filter, PVACB-8 filter was manufactured on a sensor and removed from the sensor (via dissolution in methanol) a total of 10 times. After each filter removal, the sensor was tested by measuring the mean gray value (MGV). To measure the MGV, uniform monochromatic light was projected onto the sensor array, and the image created at the sensor array was captured and with the dark frame subtracted, a mean value over all the pixels was calculated.

During the measurements the humidity and temperature conditions were kept consistent. The temperature was 23 C $\pm$ 0.1 °C and humidity 25 $\pm$ 0.2%. The location of the sensor was set and fixed to prevent light distribution and the amount of light that reaches the sensor from varying. The location of all the optical elements and the light intensity, collimation and uniformity were controlled. The exposure time, frame per second (FPS), gain and offset of the CIS were set and kept fixed during all experiments.

Equation (1) was used to calculate the variation in MGV (in percentage) relative to the value obtained in the first measurement as a function of consecutive filter removal and not dependent on wavelength. In equation (1), n is the experiment number and N_λ are the different wavelengths the MGV was measured for. We repeatedly measured the curve for wavelengths from 300 nm to 600 nm in 10 nm steps. However, since the MGV at 300 nm was constantly 0, the variation was calculated for 310 nm and up; consequently the MGV was measured for 30 different wavelengths ($N_\lambda = 30$)

$$\Delta MGV\% = \frac{\sum_\lambda \sqrt{\frac{(MGV_n(\lambda) - MGV_1(\lambda))^2}{MGV_1(\lambda)}}}{N_\lambda} \cdot 100. \tag{1}$$
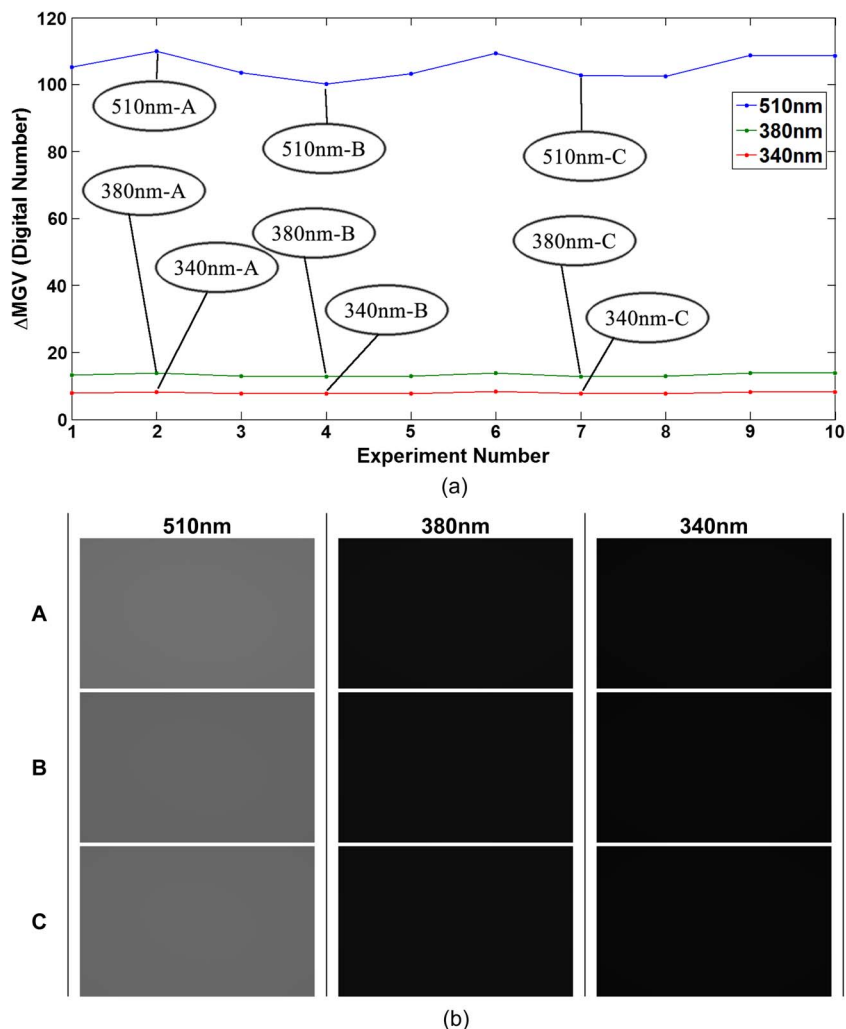
Fig. 4. The graph demonstrates the (a) variation in MGV. Specifically, it shows that there is no decline in the performance of the imager as the PVAcB-8 emission filter is applied, removed and reapplied to the sensor array over 10 experiments. (b) A sample of several images captured for MGV measurements is shown.

Selective results of MGV (for wavelengths 340 nm, 380 nm, and 510 nm) as a function of different experiments are shown in Fig. 4. The variation did not show consistent decline as a function of the amount of times the filter was applied. Instead, fluctuations occur around a mean MGV value of 105. Similar to the raw data results acquired, equation (1) did not show constant increase; instead they showed fluctuations in sensor response under 4.5%. This variation in measured MGV is due to small variation in experimental parameters, such as sensor cleanliness, location of the sensor (relative to the projected light), temperature, humidity, stray light and other parameters that affect xenon lamp output or the signal as it is perceived by the sensor.

The results from performed MGV measurements confirmed that careful use of the sensor with the manufactured filter provided repeatable results and did not degrade the performance of the system. It is important to note that for performing all of the experiments described in this work, a total of 5 UI-1222LE-M-GLs were used. For each experiment the PVAcB-8 filter was applied to the sensor (or sensors) and after the experiment, it was removed by dissolution in methanol. We calculated that on average each of the 5 sensors was reused over 10 times in total for different purposes. By using an easily removable filter, we have been able to reduce the cost of sensors to less than 10% of the total cost of the system.
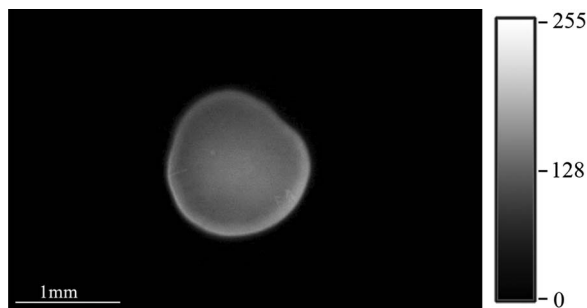
Fig. 5. The fluorescent image of a 1 μl droplet of B0200 fluorescent microspheres (2 μm diameter) in aquas solution. The droplet was excited via a 380 nm UV light and captured with the fluorescent contact imaging system.

The authors are unaware of previously published work that discusses the removal and re-application of emission filter on the sensor array. This property of the filter should not be considered as trivial since commonly used polymers (such as PDMS) are difficult to remove after polymerization [30]. It is important to note that removing the emission filter from the sensor allows us to use the sensor for any application. It is important to distinguish between cleaning the filter of pollutants (which allows reusing the system for the same purpose) to removing the filter completely.

5. System Testing With a Fluorescent Micro-model

Before testing the system with neurons, we performed additional preliminary tests. The tests were used to (1) confirmed the ability of the system to attenuate wavelengths under 400 nm, (2) test the system's ability to detect fluorescent emission above 400 nm and (3) to test repeatability of the acquired results.

For the purposes of the system, testing Duke Scientific B0200 [31] fluorescent polymer micro-spheres were used. The fluorescent microspheres are 2 μm in diameter and are in aqueous solution. The microspheres were excited via 340 nm and 380 nm light, with an emission peak wavelength of 445 nm [31].

One microliter of B0200 was transferred via a micropipette and placed on top of the CMOS sensor array in the form of a single drop. The sensor was placed underneath the excitation light and a batch of images (70 images) was captured with the image sensor. Afterwards the sensor was cleaned and reused in order to test repeatability. All the CIS settings such as exposure time, FPS, gain and offset have been set and kept fixed during all experiments.

The images were captured in two sets; a set is composed of two batches and each batch is composed of 70 images. For each batch, one microliter of B0200 was transferred via a micropipette and placed on top of the CMOS sensor array. The time interval between batch one to batch two is seven hours, the time interval between set one to set two is seven days. The images were acquired for both 340 nm and 380 nm wavelengths. A sample fluorescent image is shown in Fig. 5. A total of 280 images were captured for each 340 nm and 380 nm excitation wavelength. As can be seen from Fig. 5 the system successfully blocked excitation light and captured emission light.

For repeatability testing, the perimeter of fluorescent samples was found and the mean gray value inside the sample was calculated per image. Following the central limit theorem, the recorded MGVs have Gaussian distribution. To test that hypothesis, histograms were created for each batch and were fitted to a Gaussian curve. To show the fit quality, R-square results are shown in Table 1. From the R-squares, it can be seen that overall there is a good fit between the distributions of the mean gray value to a Gaussian distribution.

Subsequently, previously calculated mean gray values were used to test whether all of the acquired results belong to the same population. When the amount of recorded samples from two different populations is larger than 30 (from each) the Z-test statistics in equation (2) can be performed [32]. Where $\overline{x}_1$ and $\overline{x}_2$ are the means of the two recorded samples. D is the hypothesized difference, in our

TABLE 1

R-square results of Gaussian fit to histogram results of MGV values show good fit to Gaussian distribution in measuring of MGV

	380nm excitation				340nm excitation			
	Set1		Set2		Set1		Set2	
	Batch1	Batch2	Batch1	Batch2	Batch1	Batch2	Batch1	Batch2
R-square	0.99	0.98	0.99	0.97	0.93	0.99	0.95	0.99

TABLE 2

To determine repeatability of the results, the Z-score was determined for each batch. Any results under 0.0627 show good repeatability. It was shown that between the different sets of experiments, the results remained consistent and were reliable

	380nm excitation				340nm excitation			
	Set1		Set2		Set1		Set2	
	Batch1	Batch2	Batch1	Batch2	Batch1	Batch2	Batch1	Batch2
Z-Score	---------	0.0236	0.0475	0.0417	---------	0.0261	0.0252	0.0331

case D $= 0$ because the samples should belong to same population. Finally $\sigma_{(\overline{x}_1 - \overline{x}_2)}$ is given in equation (3) [32] where σ_1^2 and σ_2^2 are the variances and n_1 and n_2 are the number of sample sizes.

$$z = \frac{(\overline{x}_1 - \overline{x}_2) - D}{\sigma_{(\overline{x}_1 - \overline{x}_2)}} \tag{2}$$

$$\sigma_{(\overline{x}_1 - \overline{x}_2)} = \sqrt{\frac{\sigma_1^2}{n_1} + \frac{\sigma_2^2}{n_2}} \tag{3}$$

For z $> |1.96|$ we can reject repeatability with a certainty of 0.05, i.e. the probability for the two samples being from the same population is less than 5%. While for z $< |0.0627|$ we can conclude that with probability of 95% the two samples are from the same population (i.e., repeatability). An in between z-score test value (between 0. 0627 to 1.96) shows that we can neither confirm nor deny that whether the samples are from the same population. The z-score statistics results are in shown in Table 2. In Table 2 there is no result for Batch 1 of Set 1 because the rest of the batches were compared to it. As it can be seen from Table 2 there is good repeatability for both excitation wavelengths.

6. System Testing With Lymnaea Stagnalis Neurons

The main application of our system is to monitor fluorescence from live neurons loaded with Fura-2. To test our system, *Lymnaea stagnalis* neurons were used. The following aspects were tested: (1) the ability of the system to detect fluorescence from both 340 nm and 380 nm excitation light, (2) the ability of the system to monitor changes in intracellular calcium via changes in fluorescence from 340 nm and 380 nm excitation, (3) the ability of the system to image neurons over a wide field of view. For all three tests the same system (described in Fig. 1), same imaging parameters, same culturing methods and loading method have been used.

The Fura-2 dye (Invitrogen, F1221) was prepared by dissolving 50 μg aliquots in 10 μL of DMSO (Spectroscopic grade). The stock solution was then further diluted into our cell culture media; defined media (Serum-free 50% L-15 medium with 20 μg/mL gentamicin and added inorganic salts at mM: 40 NaCl, 1.7 KCl, 4.1 CaCl$_2$, 1.5 MgCl$_2$, and 10 HEPES, pH 7.9; Invitrogen, San Diego, CA, USA, special order).

The neurons were cultured on the sensor covered with PVAcB-8 filters and allowed to grow overnight. The following day, the cells were loaded in a 10 μM solution of Fura-2AM (cell permeable
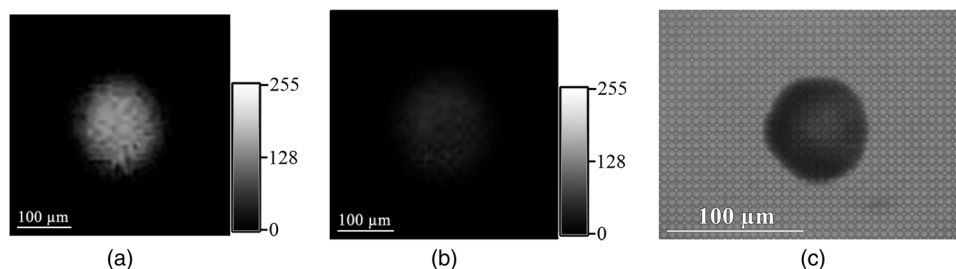
Fig. 6. Single *Lymnaea* neurons (LPeD1) were cultured onto the contact imaging chip and loaded with a Fura-2 calcium indicator. To test the fluorescence in the calcium bound and unbound state, the neuron was excited with (a) 340 nm wavelength and (b) 380 nm wavelength, respectively, and the fluorescence was detected via the image sensor. To compare the size of a single neuron relative to the individual pixels, a neuron was (c) imaged via light microscopy.

TABLE 3

Summary data showing the mean of mean of the detected fluorescent signal for both excitation wavelengths and the standard deviation for each excitation wavelength. This was conducted in a population of 9 neurons

	340nm	380nm
Mean of mean fluorescence signal	91	21
Standard deviation	20	5

variant) for 60 minutes and then washed with culture media. Contact fluorescent images of neurons were taken before and after loading Fura-2AM to control for the effects of auto-fluorescence from neurons. However, we found that no auto-fluorescence at excitation wavelengths of 340 nm and 380 nm was detected. During all the experiments the light intensity was kept constant; the integration time was kept at 500 ms (or 2 FPS), sensor gain and offset were kept at zero. The gain and offset were set to zero in order to minimize noise; the integration time was set to 500 ms for optimal contrast of fluorescence from both 340 nm and 380 nm excitation light. Though this is a relatively long integration time it is very short when compared to the excitation cycle that lasts over 200 s. If necessary the integration time could be decreased by increasing gain. The frames per second limitation of the system is imposed by the sensor which is capable to capture up to 87 frames per second [33]. The temporal resolution used in this work is superior to previous temporal resolution [17].

To test the ability of the system to detect fluorescence from both 340 nm and 380 nm excitation light, the neurons were imaged with excitation wavelengths of 340 nm and 380 nm. A sample image of single neuron is shown in Fig. 6. A total of nine neurons were tested and mean signal for each of the neurons was calculated for both excitation wavelengths by summing the fluorescent signal from each pixel within the neuron and normalizing by the area (of the neuron). Standard deviation (STD) for the signals and mean of mean were calculated and are shown in Table 3. The excitation via 340 nm yields stronger fluorescent signals. As expected the fluorescent signals have large STD due to parameters discussed in Section 5.

To test the ability of the system to monitor changes in intracellular calcium via changes in fluorescence from 340 nm and 380 nm excitation, 50 uL of 1M KCl was added locally to the 2 mL petri dish. KCl caused the neurons to depolarize and trigger action potentials, therefore causing a rise in the intracellular calcium levels of the neurons. Fluorescence was continuously recorded during and following the addition of KCl. The experiment was performed on a total of nine neurons. Fig. 7 shows a change in neuron fluorescence (versus time) as a result of KCl for four different neurons. The fluorescence is calculated as the ratio of calcium bound signal (fluorescence via 340 nm excitation) over calcium unbound signal (fluorescence via 380 nm excitation) shown in Fig. 7(a) for a

(a)
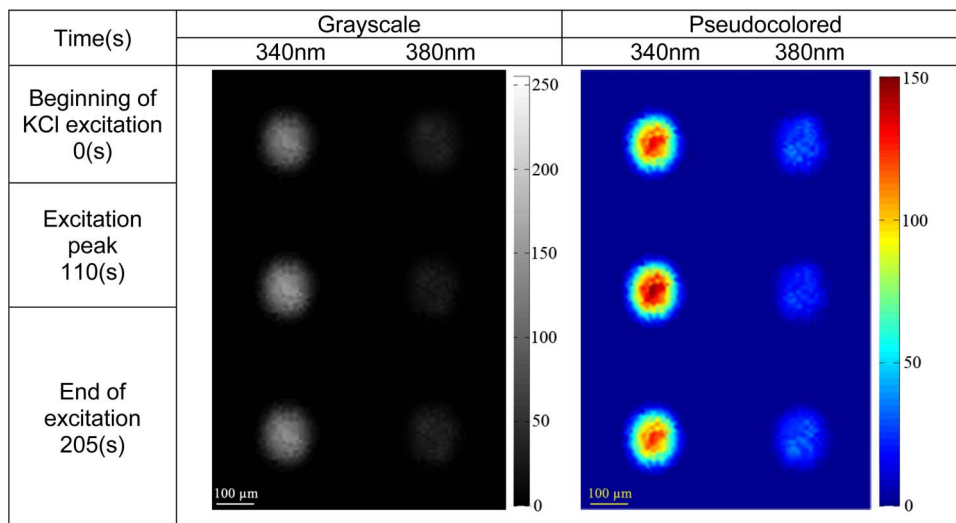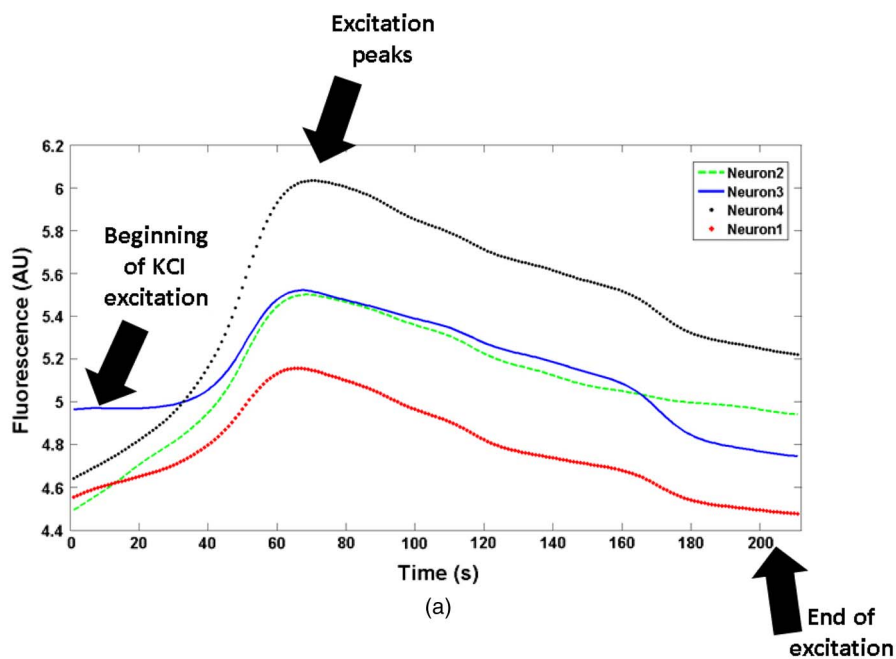
(b)

Fig. 7. To test the ability of the system to detect intracellular calcium changes, the neurons were loaded with Fura-2 calcium dye and excited with a high KCl stimulus. As shown in the figure, (a) the addition of KCl resulted in a large rise in calcium as indicated by the fluorescence change. The signal peaks at approximately 70 s following the KCl stimulus before gradually returning to baseline. (b) Sample fluorescence from a single neuron in grayscale and pseudocolor prior to KCl stimulus, at the peak of the stimulus and when returned to basal levels of calcium.

single neuron. The images as recorded from the neuron itself are shown in Fig. 7(b) both in grayscale and pseudocolor.

Finally the ability of the system to image neurons over wide field of view was tested. In conventional fluorescent microscopy, there is an inverse relation between the magnification and the imaged area. For effective light collection, high magnification oil immersion objectives are usually used, resulting in a small visible area of several hundred by several hundred micrometers. In previously reported work [17] we have used a fluorescence microscope limited by 300 um(H) $\times$ 400 um(V) field of view. In contact imaging, the field of view is limited by the size of the sensor array [19], [20], [34]–[36]. In this
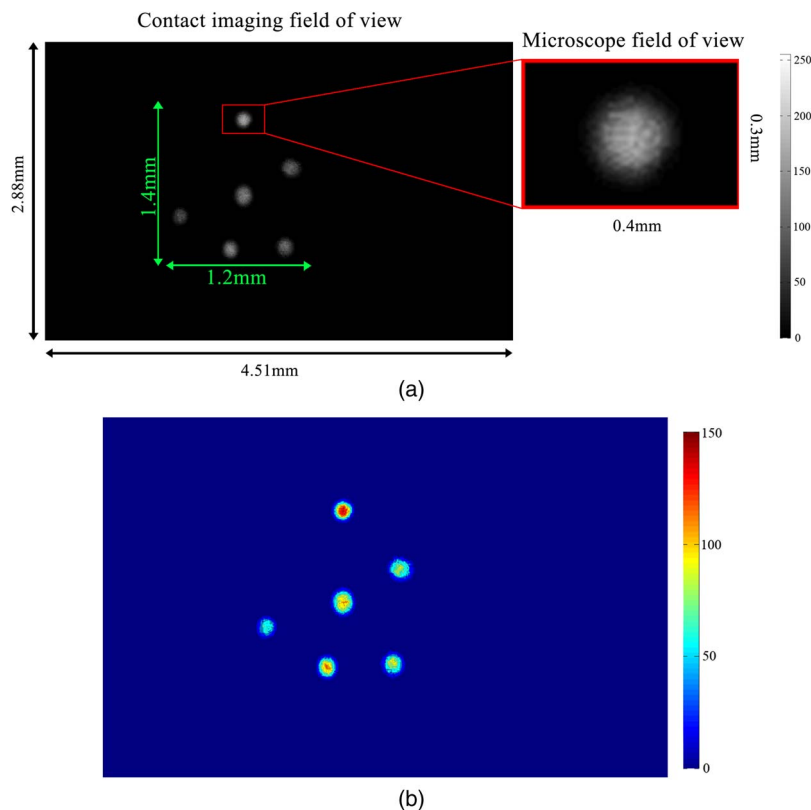
Fig. 8. To compare the field of view in a contact imaging system to a light microscopy imaging system, we show the (a) fluorescent signal of six neurons excited via 340 nm light. The red box marks an area that can be viewed by conventional fluorescence microscopy under 40× objective oil immersion imaging. The green arrows show the approximate area that is utilized by these six neurons out of the total area available. (b) Intracellular calcium concentrations can be determined for each individual neuron as seen in the fluorescence signal of six neurons excited via 340 nm light in pseudocolor.

work we are using an Aptina MT9V032 sensor with dimensions of 4.51 mm × 2.88 mm which results in a significantly increased imaging area. To demonstrate the ability of the fluorescence system to utilize a wide field of view, six neurons have been placed on top of a sensor array and loaded with Fura-2. The distance between the border neurons was measured to be 1200 um(H) × 1400 um(V). A fluorescent signal as it is captured by the whole sensor array from excitation via 340 nm light is shown in Fig. 8. In Fig. 8, the red square surrounding the upper neuron shows the field of view that can be imaged via fluorescent microscopy for comparison purposes. The authors are aware of other work [19], [20] utilizing this advantage, however it is important to note that in this work, there is no need for complicated image post processing after acquiring the fluorescent image.

7. System's Resolving Power

In this section we analyze the obtained images and determine the resolution limit of our system. Resolving power or spatial resolution limit is the minimal detail that the optical system can successfully resolve, an important parameter for any optical system. In conventional optical systems, this limit is a result of a diffraction pattern created around each imaged point at the imaging plane. This is commonly calculated by using Rayleigh criterion. In the contact imaging system, the minimal resolution is affected by other factors. For instance, one main factor is the distance between the sample and the sensor array. Additional factors include the fluorescence sample size (because it also affects the distance between the origin of fluorescence signal to the sensor array) and the fluorescence signal contrast.
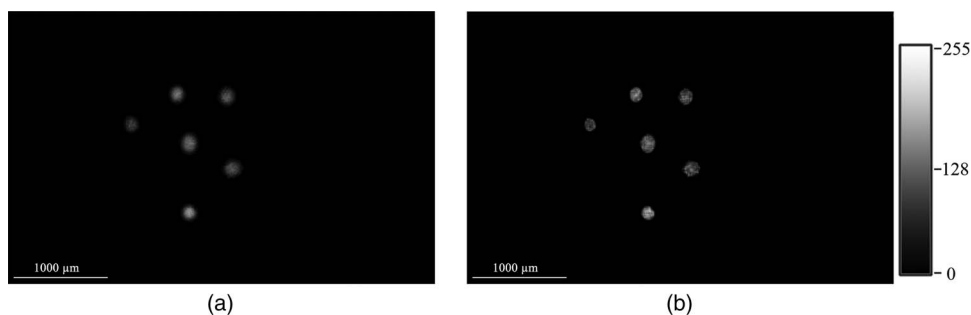
Fig. 9. The system's resolving power can be shown with deconvolution of the imaged data. This is shown in (a) before deconvolution and (b) after deconvolution.
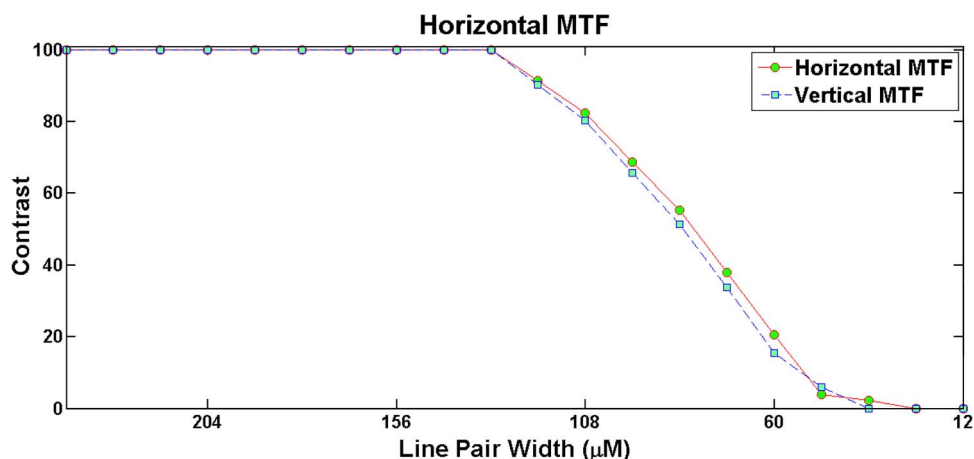

Fig. 10. Horizontal and vertical MTF calculated by convolution of step function with variable step size with PSF.

To calculate the resolution limit of our system's fluorescent signal, neurons loaded with Fura-II fluorescent dye were deconvoluted iteratively using damped Richardson-Lucy algorithm [19], [37]–[39]. Point spread function (PSF) size, shape and the amount of iterations were optimized for maximum image sharpness, maximum contrast and minimum image distortion. Point spread function errors are limited to the size of a single pixel (6 μm × 6 μm). Additionally, the PSF was optimized to the fluorescent image as a whole and not for each fluorescent sample. Optimal PSF size was calculated to be 11 pixels wide and 11 pixels high, where the size of each pixel is 6 μm × 6 μm. Sample images of the neurons before and after deconvolution is shown in Fig. 9. The horizontal and vertical modulation transfer functions (MTF) were calculated by performing convolution of PSF and a step function pattern (the step pattern was manufactured in terms of pixels, therefore each line has a multiplier of 6 and a pair of lines is a multiplier of 12). This is presented in Fig. 10.

Unfortunately, there is no single cut off criteria for the resolution limit based on the MTF curve. Hence, several cut offs have been proposed. Rayleigh claimed that a contrast of 26% is necessary, while Dawes established empirically that in some cases a contrast of only 3.2% is enough [40]. Based on the variance in the cut off criteria we have applied our PSF to a step function pattern with pair width of 48 μm and 60 μm. These line widths correspond to horizontal/vertical MTF values of 3.9%/5.8%, and 20.4%/15.3% accordingly (Fig. 11). From the presented results, we can see that the 3.9% contrast is within visual limits to recognize horizontal resolution for line pair width equal to 48 μm. However, for line pair width equaling 60 μm, after applying the PSF we can visually distinguish the pattern. Therefore, we conclude that based on the calculated PSF, the system's resolution limit is 30 μm.
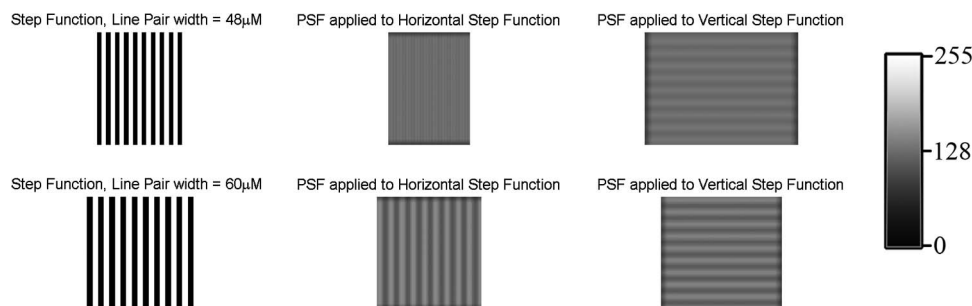
Fig. 11. PSF applied to step function pattern for observing of result contrast. From the observed result contrast line pair 60 μm is the selected cut off frequency.

8. Conclusion

In summary, here we demonstrate a complete bio-compatible fluorescence contact imaging system. The system has been tested with fluorescent micro beads and has shown strong fluorescent signal detection. Repeatability tests were performed (by using microbeads) and showed good repeatability. The system has also been tested for repetitive use by applying, removing and reapplying the filter multiple times. Each time after filter's removal the sensor's sensitivity was tested and test results showed no degradation of the sensor's performance.

The system has been tested with *Lymnaea stagnalis* neurons and can resolve fluorescence at 340 nm and 380 nm excitation light and monitor variations in the fluorescent signal. Additionally this work has demonstrated the ability of a contact fluorescence imaging system to use wide field of view in order to monitor large fluorescent samples or large quantity of fluorescent samples at the same time, without the need for complicated image post processing. The spatial resolution limit of our contact fluorescent system has been calculated to be 30 μm when imaging *Lymnaea stagnalis* neurons.

The sensor portion of the system includes a CMOS sensor, FPGA board and the sample holder (petri-dish) was measured to be 36 $\times$ 36 $\times$ 18 mm (H $\times$ W $\times$ D). The excitation light can be further reduced in size by utilizing UV LEDs.

During the tests with neurons, the integration time has been set to 500 ms, which offers sufficient temporal resolution in order to successfully monitor changes in fluorescent signal for this application. If necessary, the integration time can be further decreased by increasing the sensor's gain.

Ratiometric contact fluorescent imaging of neurons is more complicated than many other applications mainly due to two factors. These include the need for (1) two excitation wavelengths and (2) a weak fluorescent signal due to a small sample size and small fluorescent concentration. As far as the authors are aware, this is the first time that ratiometric contact fluorescent imaging is reported via live cells. These results show that contact fluorescence imaging is an effective alternative to conventional fluorescent imaging even for complicated applications. Future utility of the current technology can be in situations where conventional fluorescence microscopes fail to provide a solution. For instance, in the field of neurodevelopment, there is much information that we currently do not know regarding neuronal circuit development and the role of activity and calcium. One of the greatest limitations is that with our current technology, it is difficult to conduct long-term calcium imaging. This is due to the half-life and photobleaching of calcium indicators following long-term recordings. With contact imaging, a tightly coupled sensor allows for the detection of much lower thresholds of fluorescence in comparison to conventional microscopy. Further, because of the higher sensitivity in detection, a lower level excitation source is required to stimulate the calcium dye, increasing the longevity of the fluorophore.

The fundamental building block of the nervous system is the neuron. However, alone, a neuron is not able to account for the enormous functions that a nervous system is able to perform. Rather, it is through the complex interconnections between hundreds of billions of neurons in large networks that result in a functioning nervous system. These interconnections allow for the nervous system to control

functions from basic reflexes to locomotion, higher order cognition and learning and memory. Hence, to understand how the brain functions, it is critical that we are not only monitoring the activity of a single neuron, but to simultaneously record from multiple neurons in a neuronal network. Currently, optical systems limit the field of view and the number of neurons that can be monitored. Therefore, our current understanding of network activity is limited by the area which we can monitor. However, the significantly larger field of view provided by the contact imaging system will allow for a vastly larger network to be simultaneously interrogated. This technology allows for us to move towards the ideal situation of being able to record from the entire brain at a high resolution.

Application of this contact imaging technology can be in other situations where conventional fluorescence microscopes provide a cumbersome solution, such as fluorescence imaging of the brain in freely moving animals [41]. Contact fluorescence imaging could provide smaller, lighter wireless approaches. This would have a smaller impact on the animal and would allow viewing a larger field of view when compared to the current approaches [41]. Other possible application include monitoring fluorescence signal of water quality in remote areas where the existing commercially available devices do not employ contact technology and use fibers to deliver the excitation light and collect the emission signal. Commercial devices are mostly in a shape of a tube, their size is 20 cm length and 10 cm in diameter; their weight is 1.5 kg; the minimum power supply requirement is 5W [42], [43]. Their prices start from several thousands of dollars. Contact fluorescence approach can offer smaller and lighter devices with smaller power requirement at smaller price.

Acknowledgment

References

[1] H. Ji, D. Sander, A. Haas, and P. A. Abshire, "Contact imaging: Simulation and experiment," *IEEE Trans. Circuits Syst. I, Reg. Papers*, vol. 54, no. 8, pp. 1698–1710, Aug. 2007.

[2] K. Salama, H. Eltoukhy, A. Hassibi, and A. El-Gamal, "Modeling and simulation of luminescence detection platforms," *Biosens. Bioelectron.*, vol. 19, no. 11, pp. 1377–1386, Jun. 2004.

[3] A. Greenbaum, W. Luo, T.-W. Su, Z. Göröcs, L. Xue, S. O. Isikman, A. F. Coskun, O. Mudanyali, and A. Ozcan, "Imaging without lenses: Achievements and remaining challenges of wide-field on-chip microscopy," *Nat. Methods*, vol. 9, no. 9, pp. 889–895, Sep. 2012.

[4] N. Manaresi, A. Romani, G. Medoro, L. Altomare, A. Leonardi, M. Tartagni, and R. Guerrieri, "A CMOS chip for individual cell manipulation and detection," *IEEE J. Solid State Circuits*, vol. 38, no. 12, pp. 2297–2305, Dec. 2003.

[5] J. Ohta, T. Tokuda, K. Kagawa, M. Nunoshita, and S. Shiosaka, "Pulse modulation CMOS image sensor for bio-fluorescence imaging applications," in *Proc. IEEE Int. Symp. Circuits Syst.*, 2005, pp. 3487–3490.

[6] S. Mironov, E. Skorova, G. Taschenberger, N. Hartelt, V. Nikolaev, M. Lohse, and S. Kügler, "Imaging cytoplasmic cAMP in mouse brainstem neurons," *BMC Neurosci.*, vol. 10, p. 29, 2009.

[7] Z. Serfozo and K. Elekes, "Chemical properties of the extracellular matrix of the snail nervous system: A comprehensive study using a combination of histochemical techniques," *Micron Oxford Engl.*, vol. 41, no. 5, pp. 461–471, 2010, 1993.

[8] X. Tan, H. Liao, L. Sun, M. Okabe, Z. Xiao, and G. S. Dawe, "Fetal microchimerism in the maternal mouse brain: A novel population of fetal progenitor or stem cells able to cross the blood-brain barrier?" Stem cells Dayt. Ohio, vol. 23, no. 10, pp. 1443–1452, Nov./Dec. 2005.

[9] J. Bradley, R. Luo, T. S. Otis, and D. A. DiGregorio, "Submillisecond optical reporting of membrane potential in situ using a neuronal tracer dye," *J. Neurosci.*, vol. 29, no. 29, pp. 9197–9209, Jul. 2009.

[10] L. Tian, S. A. Hires, T. Mao, D. Huber, M. E. Chiappe, S. H. Chalasani, L. Petreanu, J. Akerboom, S. A. McKinney, E. R. Schreiter, C. I. Bargmann, V. Jayaraman, K. Svoboda, and L. L. Looger, "Imaging neural activity in worms, flies and mice with improved GCaMP calcium indicators," *Nat. Methods*, vol. 6, pp. 875–881, 2009.

[11] E. Entcheva, S. N. Lu, R. H. Troppman, V. Sharma, and L. Tung, "Contact fluorescence imaging of reentry in monolayers of cultured neonatal rat ventricular myocytes," *J. Cardiovasc. Electrophysiol.*, vol. 11, no. 6, pp. 665–676, Jun. 2000.

[12] E. Entcheva, Y. Kostov, E. Tchernev, and L. Tung, "Fluorescence imaging of electrical activity in cardiac cells using an all-solid-state system," *IEEE Trans. Biomed. Eng.*, vol. 51, no. 2, pp. 333–341, Feb. 2004.

[13] D. C. Ng, T. Tokuda, A. Yamamoto, M. Matsuo, M. Nunoshita, H. Tamura, Y. Ishikawa, S. Shiosaka, and J. Ohta, "On-chip biofluorescence imaging inside a brain tissue phantom using a CMOS image sensor for in vivo brain imaging verification," *Sens. Actuators B Chem.*, vol. 119, no. 1, pp. 262–274, Nov. 2006.

[14] C. C. Luk, H. Naruo, D. Prince, A. Hassan, S. A. Doran, J. I. Goldberg, and N. I. Syed, "A novel form of presynaptic CaMKII-dependent short-term potentiation between Lymnaea neurons," *Eur. J. Neurosci.*, vol. 34, no. 4, pp. 569–577, Aug. 2011.

[15] J. Reichman, *Handbook Of Optical Filters For Fluorescence Microscopy*. Brattleboro, VT, USA: Chroma Technology Corp., 2010.

[16] M. Sauer, H. Johan, and E. Jörg, *Handbook of Fluorescence Spectroscopy and Imaging: From Ensemble to Single Molecules*. Hoboken, NJ, USA: Wiley, 2010.

[17] L. Blockstein, C. C. Luk, a. K. Mudraboyina, N. I. Syed, and O. Yadid-Pecht, "A PVAc-Based Benzophenone-8 Filter as an Alternative to Commercially Available Dichroic Filters for Monitoring Calcium Activity in Live Neurons via Fura-2 AM," *IEEE Photon. J.*, vol. 4, no. 3, pp. 1004–1012, Jun. 2012.

[18] N. Nelson, D. Sander, M. Dandin, S. B. Prakash, A. Sarje, and P. Abshire, "Handheld Fluorometers for Lab-on-a-Chip Applications," *IEEE Trans. Biomed. Circuits Syst.*, vol. 3, no. 2, pp. 97–107, Apr. 2009.

[19] A. F. Coskun, T.-W. Su, and A. Ozcan, "Wide field-of-view lens-free fluorescent imaging on a chip," *Lab Chip*, vol. 10, no. 7, pp. 824–827, Apr. 2010.

[20] A. F. Coskun, I. Sencan, T.-W. Su, and A. Ozcan, "Lensfree fluorescent on-chip imaging of transgenic Caenorhabditis elegans over an ultra-wide field-of-view," *PLoS One*, vol. 6, no. 1, p. e15955, Jan. 2011.

[21] Aptina, *1/3-Inch Wide-VGA CMOS Digital Image Sensor,* 2005.

[22] M. Beiderman, T. Tam, A. Fish, G. A. Jullien, and O. Yadid-Pecht, "A low-light CMOS contact imager with an emission filter for biosensing applications," *IEEE Trans. Biomed. Circuits Syst.*, vol. 2, no. 3, pp. 193–203, Sep. 2008.

[23] Y. Dattner and O. Yadid-Pecht, "Low light CMOS contact imager with an integrated poly-acrylic emission filter for fluorescence detection," *Sensors*, vol. 10, no. 5, pp. 5014–5027, 2010, (Peterboroug).

[24] R. R. Singh, D. Ho, A. Nilchi, G. Gulak, P. Yau, and R. Genov, "A CMOS / thin-film fluorescence contact imaging microsystem for DNA analysis," *IEEE Trans. Circuits Syst. I, Reg. Papers*, vol. 57, no. 5, pp. 1029–1038, May 2010.

[25] D. Ho, M. O. Noor, U. J. Krull, G. Gulak, and R. Genov, "Single-filter multi-color CMOS fluorescent contact sensing microsystem," in *Proc. IEEE ISCAS*, 2012, pp. 2393–2396.

[26] O. Hofmann, X. Wang, A. Cornwell, S. Beecher, A. Raja, D. D. C. Bradley, A. J. Demello, and J. C. Demello, "Monolithically integrated dye-doped PDMS long-pass filters for disposable on-chip fluorescence detection," *Lab Chip*, vol. 6, pp. 981–987, 2006.

[27] Y.-H. Kim, K.-S. Shin, J.-Y. Kang, E.-G. Yang, K.-K. Paek, D.-S. Seo, and B.-K. Ju, "Poly(dimethylsiloxane)-based packaging technique for microchip fluorescence detection system applications," *J. Microelectromech. Syst.*, vol. 15, no. 5, pp. 1152–1158, Oct. 2006.

[28] C. Richard, A. Renaudin, V. Aimez, and P. G. Charette, "An integrated hybrid interference and absorption filter for fluorescence detection in lab-on-a-chip devices," *Lab Chip*, vol. 9, pp. 1371–1376, 2009.

[29] H. Ji, M. Dandin, P. Abshire, and E. Smela, "Integrated fluorescence sensing for lab-on-a-chip devices," in *Proc. Life Sci. Syst. Appl. Workshop*, 2006, pp. 1–2.

[30] J. N. Lee, C. Park, and G. M. Whitesides, "Solvent compatibility of poly (dimethylsiloxane)-based microfluidic devices," *Anal. Chem.*, vol. 75, no. 23, pp. 6544–6554, Dec. 2003.

[31] Duke Scientific Corporation, *Fluorescent Polymer Microspheres,* 2005.

[32] J. T. McClave and F. H. Dietritch, *Statistics*, 5th ed. San Francisco, CA, USA: Dellen Publishing Company, 1991, pp. 334, 381–382.

[33] 1stVision, *UI-122xLE Datasheet,* 1–8 (n.d.)

[34] A. F. Coskun, I. Sencan, T.-W. Su, and A. Ozcan, "Lensless wide-field fluorescent imaging on a chip using compressive decoding of sparse objects," *Opt. Exp.*, vol. 18, no. 10, pp. 10510–10523, May 2010.

[35] A. F. Coskun, I. Sencan, T.-W. Su, and A. Ozcan, "Wide-field lensless fluorescent microscopy using a tapered fiber-optic faceplate on a chip," *Analyst*, vol. 136, no. 17, pp. 3512–3518, Sep. 2011.

[36] A. F. Coskun, T.-W. Su, I. Sencan, and A. Ozcan, "Lensless fluorescent microscopy on a chip," *J. Vis. Exp.*, vol. 54, p. e3181, Aug. 2011.

[37] T. J. Holmes and Y. H. Liu, "Richardson-Lucy/maximum likelihood image restoration algorithm for fluorescence microscopy: Further testing," *Appl. Opt.*, vol. 28, no. 22, pp. 4930–4938, Nov. 1989.

[38] W. H. Richardson, "Bayesian-based iterative method of image restoration," *J. Opt. Soc. Amer.*, vol. 62, no. 1, pp. 55–59, Jan. 1972.

[39] D. A. Fish, A. M. Brinicombe, E. R. Pike, and J. G. Walker, "Blind deconvolution by means of the Richardson–Lucy algorithm," *J. Opt. Soc. Amer. A*, vol. 12, no. 1, pp. 58–65, 1995.

[40] H. G. J. Rutten and M. A. M. Van Venrooij, *Telescope Optics Complete Manual for Amateur Astronomers*. Richmond, VA, USA: Willmann-Bell, 1988, p. 214.

[41] J. N. Kerr and A. Nimmerjahn, "Functional imaging in freely moving animals," *Curr. Opin. Neurobiol.*, vol. 22, no. 1, pp. 45–53, Feb. 2012.

[42] Turner Designs, *C3 Submersible Fluorometer.*

[43] YSI, YSI 6600. [Online]. Available: http://www.ysi.com/media/pdfs/E52-6600V2.pdf